Giant Frictional Drag in Double Bilayer Graphene Heterostructures

Kayoung Lee,[1] Jiamin Xue,[1] David C. Dillen,[1] Kenji Watanabe,[2] Takashi Taniguchi,[2] and Emanuel Tutuc[1]
[1]Microelectronics Research Center, The University of Texas at Austin, Austin, Texas 78758, USA
[2]National Institute of Materials Science, 1-1 Namiki Tsukuba, Ibaraki 305-0044, Japan
(Received 28 February 2016; published 18 July 2016)

We study the frictional drag between carriers in two bilayer graphene flakes separated by a 2–5 nm thick hexagonal boron nitride dielectric. At temperatures (T) lower than ~10 K, we observe a large anomalous negative drag emerging predominantly near the drag layer charge neutrality. The anomalous drag resistivity increases dramatically with reducing T, and becomes comparable to the layer resistivity at the lowest $T = 1.5$ K. At low T the drag resistivity exhibits a breakdown of layer reciprocity. A comparison of the drag resistivity and the drag layer Peltier coefficient suggests a thermoelectric origin of this anomalous drag.

DOI: 10.1103/PhysRevLett.117.046803

Interaction between isolated electron systems in close proximity can produce a wealth of novel phenomena. A particularly striking example is frictional drag, where charge current (I_{Drive}) flowing in one (drive) layer induces a voltage drop in the opposite (drag) layer, $V_{\mathrm{Drag}} = R_D I_{\mathrm{Drive}}$. At the heart of the transresistance R_D are interlayer couplings without particle exchange which can be mediated by, e.g., momentum exchange [1], energy transfer [2], or phonons [3]. While being a sensitive probe of interlayer interactions, the R_D values are generally much smaller than the layer resistance. An exception occurs when the carriers in the two layers form a correlated state, yielding R_D's that can reach values comparable to the layer resistance. Indeed, this has been experimentally reported in GaAs electron [4], or hole [5] double layer systems, in magnetic fields such that each layer has one half-filled Landau level [6].

Extensive experimental effort has been devoted to probing drag in electron-hole double layers, using GaAs electron-hole double layers [7,8], graphene double layers [9,10], and, most recently, graphene-GaAs double layers [11], motivated in part by the search for equilibrium indirect exciton condensates. A common thread in these experiments is an anomalous R_D that increases with reducing T, along with a breakdown of layer reciprocity when interchanging the drive and drag layers [7,8,11]. In this regard, double bilayer graphene separated by a thin hexagonal boron nitride (hBN) is a particularly compelling system. The near parabolic energy-momentum dispersion in bilayer graphene allows the Coulomb to kinetic energy ratio to be tuned via density, unlike monolayer graphene, where this ratio is fixed [12]. Moreover, the availability of ultrathin dielectrics allows double layers to be realized with interlayer spacing (d) down to a few nanometers, granting access to the strong coupling regime $d \ll l$, where l is the interparticle distance. This effectively nests the two isolated electronic systems in the same plane. Here, we investigate the frictional drag in double bilayer graphene heterostructures, consisting of two bilayer graphene separated by a 2–5 nm thick interlayer hBN dielectric, which allows us to explore the drag in a wide range of layer densities and for all combinations of carrier polarity. Strikingly, we find a giant and negative drag resistivity at charge neutrality, comparable to the layer resistivity at the lowest T.

The samples [Fig. 1(a)] are fabricated using a layer-by-layer transfer process similar to samples discussed in Ref. [13]. The layer densities are tuned using a combination of back-gate (V_{BG}), and interlayer bias applied on the top bilayer (V_{TL}) [14]. The top (ρ_T) and bottom (ρ_B) bilayer resistivities, as well as the frictional drag, are probed using small signal, low frequency lock-in techniques. We investigated five samples, labeled A–E, with different interlayer spacing and layer mobilities. The interlayer resistance values are in the range 1.6–20 GΩ. The drag resistance measurement errors associated with finite interlayer resistance are on the order of 1%. The key features of the drag data discussed below are similar in all samples.

Figures 1(b) and 1(c) show ρ_B and ρ_T measured in sample A at $T = 1.5$ K. The bottom bilayer responds to V_{BG} and V_{TL} similarly to a dual-gated bilayer graphene, in which the density and transverse electric field (E) are controlled independently [15]. The locus of high resistance points in Figs. 1(b) and 1(c) marks the charge neutrality lines for both bilayers. Figure 1(c) also shows the carrier type in each of the four quadrants defined by the two charge neutrality lines. To examine variations in the drag resistance when interchanging the drag and drive layers, we probe both the bottom ($\rho_{D,B}$) and top ($\rho_{D,T}$) drag resistivities, with the top and bottom bilayers serving as the drive layers, respectively. Figures 1(d) and 1(e) show $\rho_{D,B}$ and $\rho_{D,T}$, respectively, measured as a function of V_{BG} and V_{TL} in sample A, at $T = 1.5$ K. A comparison of data from Figs. 1(b) and 1(c), on one hand, and data from Figs. 1(d) and 1(e), on the other, shows a large, negative drag

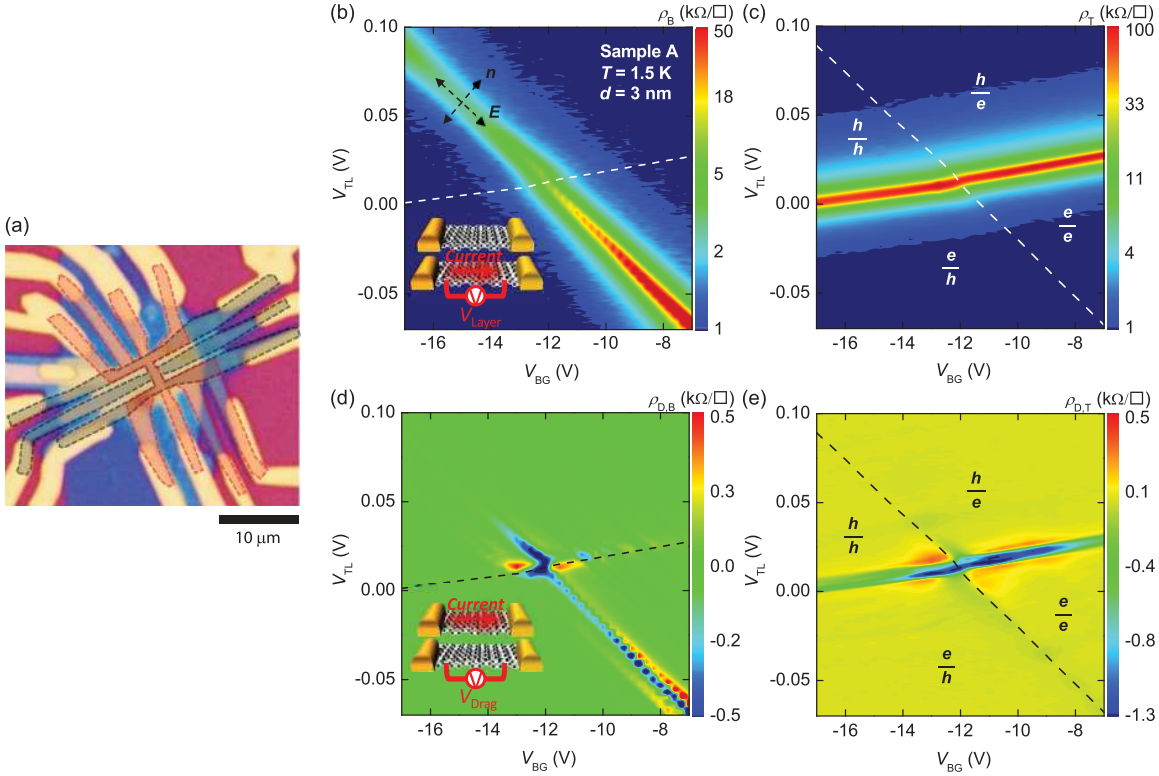

FIG. 1. (a) Optical micrograph of a double bilayer graphene heterostructure. The red (gray) dashed contour lines mark the top (bottom) bilayer. (b) ρ_B, and (c) ρ_T measured in sample A as a function of V_{BG} and V_{TL} at $T = 1.5$ K. The inset in (b) shows the sample and measurement schematic. The white dashed lines in (b) and (c) mark the charge neutrality lines of the top and bottom bilayers, respectively. (d) $\rho_{D,B}$ and (e) $\rho_{D,T}$ measured as a function of V_{BG} and V_{TL} at $T = 1.5$ K. The carrier type in the two bilayers are indicated in panels (c) and (e), in the four quadrants defined by the two charge neutrality lines.

resistivity emerging predominantly near or at the drag layer charge neutrality.

To better visualize the data in Figs. 1(d) and 1(e), we plot $\rho_{D,B}$ [Fig. 2(a)] and $\rho_{D,T}$ [Fig. 2(b)] as a function of top (n_T) and bottom (n_B) bilayer densities, converted from V_{BG} and V_{TL}. The n_T and n_B values are related to the applied V_{BG} and V_{TL} biases, referenced with respect to $n_B = n_T = 0$, via $eV_{\mathrm{BG}} = e^2(n_B + n_T)/C_{\mathrm{BG}} + \mu_B$ and $eV_{\mathrm{TL}} = -e^2 n_T/C_{\mathrm{int}} + \mu_B - \mu_T$, where C_{BG} and C_{int} are the back-gate and interlayer capacitances, μ_T and μ_B are the top and bottom bilayer chemical potentials, respectively, and e is the electron charge. To convert V_{BG} and V_{TL} to layer densities, we use the density-dependent chemical potential determined experimentally [13]. The C_{BG} and C_{int} values are determined using magnetotransport measurements of individual bilayers [16]. Figure 2 reveals a number of interesting features. First, $\rho_{D,B}$ is large in the proximity of the $n_B = 0$ line in Fig. 2(a), while $\rho_{D,T}$ is large near the $n_T = 0$ line in Fig. 2(b). Near the double neutrality point (DNP), $n_B = n_T = 0$, $\rho_{D,B}$ and $\rho_{D,T}$ reach values close to 1 kΩ. Second, the reciprocity with respect to interchanging the drag and drive layers breaks down, i.e., $\rho_{D,B}(n_B, n_T) \neq \rho_{D,T}(n_B, n_T)$ in Fig. 2.

In light of the anomalous drag observed in Figs. 1 and 2, in the following we examine the drag layer resistivity in more detail, concentrating on the drag layer density and E dependencies. The latter is relevant for bilayer graphene as the energy-momentum dispersion changes with E, concomitant with gap opening at charge neutrality [17]. Figure 3(a) shows sample A ρ_B, $\rho_{D,B}$, and the corresponding normalized drag $\rho_{D,B}/\rho_B$ as a function of $n_B = -n_T$, namely, at equal density in the two bilayers, with opposite carrier polarity. $\rho_{D,B}$ shows a very strong, negative peak at the DNP, which, surprisingly, becomes comparable to ρ_B at

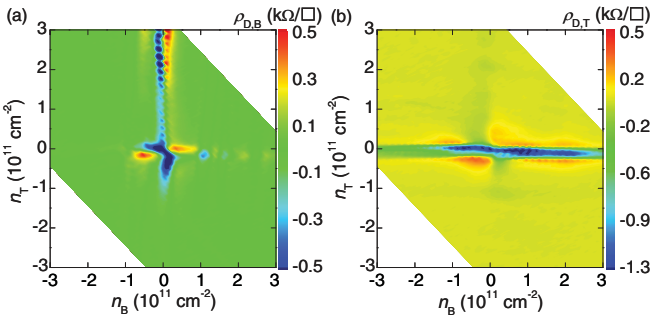

FIG. 2. (a) $\rho_{D,B}$ and (b) $\rho_{D,T}$ as a function of n_B and n_T, measured at $T = 1.5$ K. The data show a large drag resistivity emerging along the drag layer charge neutrality, relatively insensitive to the drive layer density.

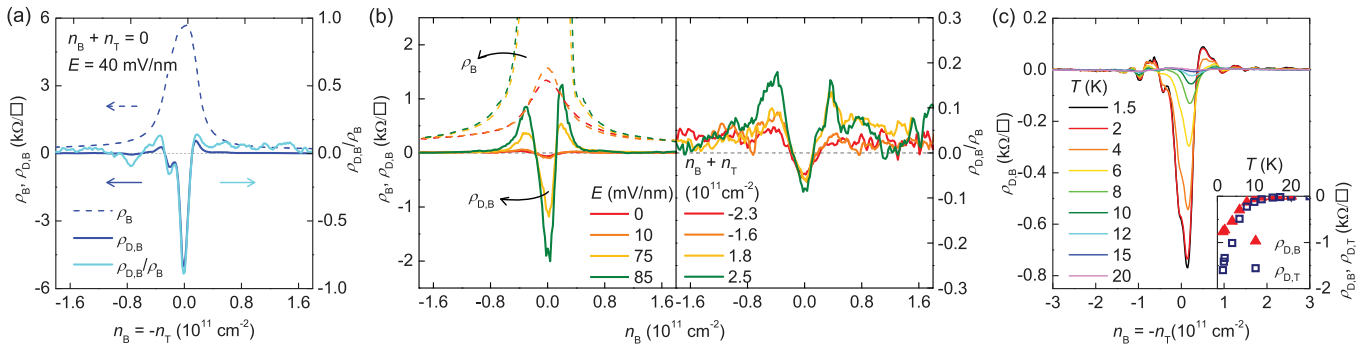

FIG. 3. (a) ρ_B, $\rho_{D,B}$ (left axis), and $\rho_{D,B}/\rho_B$ (right axis) as a function of $n_B = -n_T$, measured at $T = 1.5$ K in sample A. The $\rho_{D,B}$ and ρ_B values are comparable at the DNP. The E field across the bottom bilayer (drag layer) is 40 mV/nm at the DNP. (b) The left panel shows ρ_B (the dashed lines) and $\rho_{D,B}$ (the solid lines) vs n_B in sample A at different E values in the bottom bilayer at $T = 1.5$ K. (Right panel) $\rho_{D,B}/\rho_B$ vs n_B corresponding to the left panel data. The data were acquired at constant $n_B + n_T$ total density values. (c) $\rho_{D,B}$ as a function of $n_B = -n_T$, in the proximity of the DNP at different T, measured in sample A in a separate cooldown. (Inset) $\rho_{D,B}$ and $\rho_{D,T}$ vs T at the DNP.

$T = 1.5$ K. As $n_B = -n_T$ increases, $\rho_{D,B}$ changes sign, becomes positive at a finite $|n_B|$, then vanishes as $|n_B|$ increases further.

Figure 3(b) shows (left panel) ρ_B, $\rho_{D,B}$ and (right panel) $\rho_{D,B}/\rho_B$ vs n_B in the proximity of $n_B = 0$ and $n_T \neq 0$. The negative $\rho_{D,B}$ at $n_B = 0$ is notable, similar to the large, negative $\rho_{D,B}$ peak at the DNP in Fig. 3(a). However, the magnitude of $\rho_{D,B}/\rho_B$ at $n_B = 0$ and $n_T \neq 0$ is smaller than that at the DNP. As $|n_B|$ increases, $\rho_{D,B}$ changes polarity and becomes positive, consistent with the observed trend near the DNP, albeit with a lower magnitude. An examination of the electrostatics in double layers shows that, at $n_B = 0$, the E value across the bottom bilayer changes as n_T changes, as indicated in the Fig. 3(b) legend (see the Supplemental Material [18]). We observe that $\rho_{D,B}$ at $n_B = 0$ grows as ρ_B increases with an increasing E field, leading to a relatively constant $\rho_{D,B}/\rho_B$ ratio.

Figure 3(c) shows $\rho_{D,B}$ as a function of $n_B = -n_T$ at different T in sample A, showing a large, negative drag at the DNP. We note that Figs. 3(a) and 3(b) data were collected in one cooldown, while Fig. 3(c) data were collected in a separate cooldown. Similar to the Fig. 3(a) data, $\rho_{D,B}$ becomes positive as $|n_B|$ increases, and it subsequently decreases towards zero with an increasing density. The inset of Fig. 3(c) summarizes the T dependence of the negative peak of both $\rho_{D,B}$ and $\rho_{D,T}$ at the DNP, showing a decrease of the drag resistivity with increasing T. At the lowest T, mesoscopic fluctuations [14] are also noticeable in the proximity of the DNP in Fig. 3(c), superimposed onto the large negative drag.

The experimental observations in Figs. 1–3 have several anomalous features at variance with existing Coulomb drag theories. It is tempting to interpret the giant drag that develops at the DNP at low T as a signature of a correlated state of the two layers, such as the indirect exciton condensation. However, the fact that the drag voltage is negative—namely, opposite of the voltage drop along the drive layer—coupled with the layer reciprocity breakdown may cast doubt on this interpretation. Moreover, the increasing ρ_D observed with decreasing T [Fig. 3(c)] is the opposite of the expected dependence for momentum transfer mediated drag [1]. The increasing drag at the lowest T, coupled with the apparent breakdown of reciprocity bears similarity to the data reported in electron-hole double layers in GaAs-AlGaAs [7] or GaAs-graphene heterostructures [11]. We note that the interlayer separations in Refs. [7,11] were larger than 10 nm, and the magnitude of the measured drag resistivity was 2 orders of magnitude smaller than the values probed in the double bilayer graphene heterostructures investigated here. Indeed, the $\rho_{D,B} \approx \rho_B$ is a dramatic signature of the strong coupling regime in double layers.

To gain insight into the origin of the anomalous drag, we first note that the $\rho_{D,B}$ and ρ_B peaks in Fig. 3(a) have similar widths. The giant peak at the DNP is reminiscent of energy drag near charge neutrality in double monolayer graphene heterostructures [2,10], where Coulomb mediated vertical energy transfer coupled with correlated density inhomogeneity in the two layers yields a drag resistivity of thermoelectric origin, with the polarity determined by interlayer correlations $\langle \delta\mu_B \delta\mu_T \rangle$. To assess the role of thermoelectricity in our measurements, we use the Mott relation for the Peltier coefficient [19,20]:

$$Q = \frac{\pi^2 k_B^2 T^2}{3e} \frac{\partial\sigma/\partial\mu}{\sigma}, \tag{1}$$

where k_B is the Boltzmann constant, and σ the layer conductivity. Using Eq. (1) along with $\sigma = 1/\rho_B$ measured in the bottom bilayer graphene, the experimental μ vs n_B data (Fig. S3 in Ref. [18]), and n_B vs V_{BG} and V_{TL} (Fig. S4 in Ref. [18]), we obtain Q_B vs μ_B.

In Fig. 4(a) (main panel) we compare the drag layer chemical potential (μ_{Drag}) dependence of ρ_D and drag layer

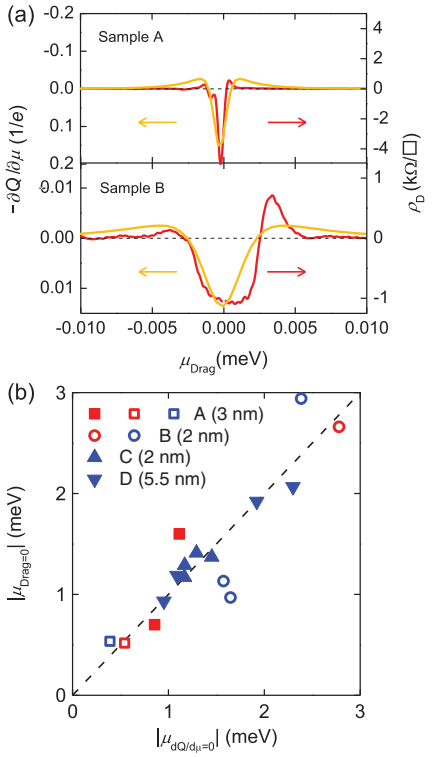

FIG. 4. (a) Drag layer $-\partial Q/\partial\mu$ (yellow) and ρ_D (red) vs μ_{Drag} in samples A and B at $T = 1.5$ K. The data were acquired by sweeping the layer densities such that $n_B = -n_T$. (b) $|\mu_{\mathrm{Drag}=0}|$ as a function of $|\mu_{dQ/d\mu=0}|$ of the drag layer for four samples, with different interlayer spacing shown in the legend. The open (closed) symbols mark data measured using the top (bottom) bilayer as drag layer. The red (blue) symbols represent data measured at zero (finite) drive layer density.

$-\partial Q/\partial\mu$ in samples A and B at $T = 1.5$ K. The bottom (top) layer serves as drag layer in sample A (B). The data were measured while sweeping the layer densities such that $n_B = -n_T$. A main difference between the two samples is that the drag layer mobility is 260 000 $\mathrm{cm}^2/\mathrm{V\,s}$ in sample A, as opposed to 19 000 $\mathrm{cm}^2/\mathrm{V\,s}$ in sample B. Remarkably, both ρ_D and $-\partial Q/\partial\mu$ show a peak at charge neutrality, change polarity as $|\mu_{\mathrm{Drag}}|$ increases, and vanish at even larger $|\mu_{\mathrm{Drag}}|$ values. Interestingly, the peak structure of energy drag in Ref. [2] arises from $\partial Q/\partial\mu$.

The similarity between the μ_{Drag} dependence of ρ_D and $-\partial Q/\partial\mu$ suggests a thermoelectric origin for the large frictional drag observed at low T in our double bilayer graphene. To further test this hypothesis, in Fig. 4(b) we compare the μ_{Drag} value at which ρ_D changes polarity ($|\mu_{\mathrm{Drag}=0}|$), and the μ value at which the drag layer $\partial Q/\partial\mu$ changes its polarity ($|\mu_{dQ/d\mu=0}|$) for multiple samples. The $|\mu_{\mathrm{Drag}=0}|$ and $|\mu_{dQ/d\mu=0}|$ are averaged over the μ values on both electron and hole branches, and they represent the half width of the ρ_D peak and the drag layer $\partial Q/\partial\mu$ peak, respectively. The $|\mu_{\mathrm{Drag}=0}|$ and $|\mu_{dQ/d\mu=0}|$ values are determined using frictional drag or layer resistance measurements in either bottom or top bilayer graphene from four samples with different interlayer thicknesses and layer mobilities. Furthermore, the data are collected at different drive layer densities, not only at the DNP. Figure 4(b) clearly indicates that $|\mu_{\mathrm{Drag}=0}|$ agrees very well with $|\mu_{dQ/d\mu=0}|$, suggesting that the overall behavior of the anomalous drag at low T is governed by the drag layer $\partial Q/\partial\mu$. Consistent with the data from Figs. 1 and 2, we do not find a correlation between the drag resistivity and the drive layer $\partial Q/\partial\mu$.

While reminiscent of energy drag, the giant drag measured here deviates from the simple energy drag picture presented in Ref. [2]. We note that Ref. [2] assumes fully overlapping layers with identical geometries and contact configurations. In contrast, in the actual devices examined here, the geometry and contact configurations of the drive or drag layers are different [Fig. 1(a)]. As a result, anisotropic heat flow due to sample geometry [21] as well as Peltier heating outside of the active layers may contribute to the layer nonreciprocity in our drag measurements. A second ingredient that may lead to nonreciprocity is the drive current-induced density gradient in both layers proportional to C_{int}, as well as to drive layer resistivity. The charge density gradient is not symmetric when interchanging the drive and drag layers, and it is largest when the layer with the lower density is used as a drive layer.

The polarity of the energy drag is determined by the sign of potential fluctuations in graphene, $\langle\delta\mu_B\delta\mu_T\rangle$ [2]. A negative drag of thermoelectric origin measured at the DNP indicates that $\langle\delta\mu_B\delta\mu_T\rangle < 0$. This suggests that strain [22], rather than charged impurities [23], dominates the density inhomogeneity. For impurity induced inhomogeneity $\langle\delta\mu_B\delta\mu_T\rangle > 0$, and a positive drag is expected at charge neutrality.

Last, we discuss similarities and differences between the energy drag previously observed in double monolayer graphene heterostructures [10,24], and the drag in double bilayer graphene heterostructures. The drag in monolayer graphene shows a peak at the DNP, has a positive value, and is maximum at higher temperatures, $T \simeq 70$ K. The positive drag at the DNP is understood as energy drag where impurity induced disorder creates a positive correlation of the layer chemical potential fluctuations $\langle\delta\mu_B\delta\mu_T\rangle$ [2]. Interestingly, a comparison of the monolayer and bilayer graphene Peltier coefficients using Eq. (1) shows that the higher density of states and smaller σ at charge neutrality in bilayer graphene yields a much larger $\partial Q/\partial\mu$, and consequently a larger drag at charge neutrality by comparison to monolayer graphene, in agreement with the experimental observations (see the Supplemental Material [18]).

In summary, we report an anomalous giant, negative frictional drag $\simeq 1$ kΩ in high mobility double bilayer graphene near the drag layer charge neutrality at temperatures lower than 10 K, with values approaching the layer resistivity at DNP. The drag increases with decreasing T

down to $T = 1.5$ K and does not obey the layer reciprocity. This opens an unanticipated playground for exploring new electron-interaction mediated phenomena in double layer systems even at zero field.

This work was supported by the SRC Nanoelectronics Research Initiative, Intel Corp, and National Science Foundation Grant No. EECS-1610008. We thank Justin Song, and Allan MacDonald for the illuminating discussions, and Sooel Son for the technical assistance.

Note added.—Recently, we became aware of the related work described in Ref. [25].

[1] P. M. Solomon, P. J. Price, D. J. Frank, and D. C. La Tulipe, Phys. Rev. Lett. **63**, 2508 (1989); T. J. Gramila, J. P. Eisenstein, A. H. MacDonald, L. N. Pfeiffer, and K. W. West, Phys. Rev. Lett. **66**, 1216 (1991).
[2] J. C. W. Song and L. S. Levitov, Phys. Rev. Lett. **109**, 236602 (2012).
[3] H. Noh, S. Zelakiewicz, T. J. Gramila, L. N. Pfeiffer, and K. W. West, Phys. Rev. B **59**, 13114 (1999).
[4] M. Kellogg, I. B. Spielman, J. P. Eisenstein, L. N. Pfeiffer, and K. W. West, Phys. Rev. Lett. **88**, 126804 (2002).
[5] E. Tutuc, M. Shayegan, and D. A. Huse, Phys. Rev. Lett. **93**, 036802 (2004).
[6] J. P. Eisenstein and A. H. MacDonald, Nature (London) **432**, 691 (2004).
[7] A. F. Croxall, K. Das Gupta, C. A. Nicoll, M. Thangaraj, H. E. Beere, I. Farrer, D. A. Ritchie, and M. Pepper, Phys. Rev. Lett. **101**, 246801 (2008).
[8] J. A. Seamons, C. P. Morath, J. L. Reno, and M. P. Lilly, Phys. Rev. Lett. **102**, 026804 (2009).
[9] S. Kim, I. Jo, J. Nah, Z. Yao, S. K. Banerjee, and E. Tutuc, Phys. Rev. B **83**, 161401(R) (2011).
[10] R. V. Gorbachev, A. K. Geim, M. I. Katsnelson, K. S. Novoselov, T. Tudorovskiy, I. V. Grigorieva, A. H. MacDonald, K. Watanabe, T. Taniguchi, and L. A. Ponomarenko, Nat. Phys. **8**, 896 (2012).
[11] A. Gamucci *et al.*, Nat. Commun. **5**, 5824 (2014).
[12] A. Perali, D. Neilson, and A. R. Hamilton, Phys. Rev. Lett. **110**, 146803 (2013).
[13] K. Lee, B. Fallahazad, J. Xue, D. C. Dillen, K. Kim, T. Taniguchi, K. Watanabe, and E. Tutuc, Science **345**, 58 (2014).
[14] S. Kim and E. Tutuc, Solid State Commun. **152**, 1283 (2012).
[15] K. Lee, B. Fallahazad, H. Min, and E. Tutuc, IEEE Trans. Electron Devices **60**, 103 (2013).
[16] B. Fallahazad *et al.*, Nano Lett. **15**, 428 (2015).
[17] E. McCann and V. I. Fal'ko, Phys. Rev. Lett. **96**, 086805 (2006).
[18] See Supplemental Material at http://link.aps.org/supplemental/10.1103/PhysRevLett.117.046803 for calculations of carrier density and E-field in a double bilayer graphene heterostructure, and expected difference in energy drag between monolayer, and bilayer graphene.
[19] N. W. Ashcroft and N. D. Mermin, *Solid State Physics* (Brooks-Cole, Belmont, MA, 1976).
[20] Y. M. Zuev, W. Chang, and P. Kim, Phys. Rev. Lett. **102**, 096807 (2009).
[21] J. C. W. Song and L. S. Levitov, Phys. Rev. Lett. **111**, 126601 (2013).
[22] M. Gibertini, A. Tomadin, F. Guinea, M. I. Katsnelson, and M. Polini, Phys. Rev. B **85**, 201405 (2012).
[23] J. Xue, J. Sanchez-Yamagishi, D. Bulmash, P. Jacquod, A. Deshpande, K. Watanabe, T. Taniguchi, P. Jarillo-Herrero, and B. J. LeRoy, Nat. Mater. **10**, 282 (2011).
[24] M. Titov *et al.*, Phys. Rev. Lett. **111**, 166601 (2013).
[25] J. I. A. Li, T. Taniguchi, K. Watanabe, J. Hone, A. Levchenko, and C. R. Dean, preceding Letter, Phys. Rev. Lett. **117**, 046802 (2016).